THE JOURNAL OF PHYSICAL CHEMISTRY C
A JOURNAL OF THE AMERICAN CHEMICAL SOCIETY

pubs.acs.org/JPCC

Article

Molecular Engineering of Water-Soluble Oligomers to Elucidate Radical π−Anion Interactions in n-Doped Nanoscale Objects

Victor Paulino, Arindam Mukhopadhyay, Ifigeneia Tsironi, Kaixuan Liu, Dalia Husainy, Chuan Liu, Katlyn Meier,* and Jean-Hubert Olivier*

Cite This: J. Phys. Chem. C 2021, 125, 10526−10538

Read Online

ACCESS | Metrics & More | Article Recommendations | Supporting Information

ABSTRACT: Modulating, by design, the electronic properties of nanoscale objects that are water-compatible is at the forefront to develop redox-responsive materials capable of interfacing and probing living organisms. In the present work, we report the synthesis and structural and electronic characterizations of two novel water-soluble naphthalene diimide (NDI) oligomers that differ in the nature of the flexible chemical linkages tethering the π-conjugated cores. Ground-state electronic absorption spectroscopy experiments, performed as a function of oligomer concentration in an aqueous medium, reveal negligible interactions between oligomer chains but significant interactions among NDI units that comprise a single oligomer chain. Contrasting the monomer controls, which demonstrate well-resolved first and second reduction processes, the NDI oligomers exhibit complex redox processes suggesting the screening of injected charges in the oligomer chains. We show that the flexible chemical linkages offer a synthetic handle to stabilize the first reduction potentials by more than 325 mV when compared to monomer controls. Because the electronic structures of these water-soluble oligomers are characterized by low-lying reduction potentials ($E^{0/-}$ = −0.025 V vs SCE), biologically relevant sacrificial electron donors, sodium ascorbate and sodium hydrosulfide, possess sufficient driving force to incrementally n-dope the NDI oligomers. Further supported by spectroelectrochemical measurements and time-dependent density functional theory (TD-DFT) calculations, the spectroscopic properties of the reduced NDI units indicate the emergence of novel spectroscopic states diagnostic of radical π−anion interactions. The existence of delocalized electron spin density is unraveled by electron paramagnetic resonance spectroscopy and is shown to be dependent on the strength of the sacrificial electron donors used to n-dope the NDI oligomer chains. Our results not only deliver new insights into the spectroscopic signatures that allow for tracking π−anion interactions in NDI-derived superstructures but also provide new avenues to tune electron spin properties in water-soluble nanoscale objects.

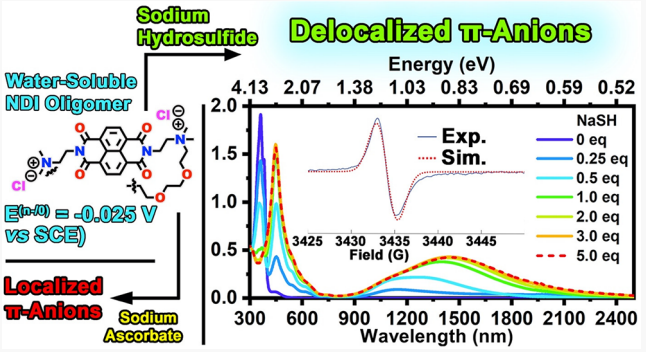

1. INTRODUCTION

Controlling the redox and electron spin properties of nanoscale objects is fueled by an interest to tailor the electronic functions of semiconducting materials.[1−5] While covalent bonds ensure the electronic coupling between π-conjugated units in conducting and semiconducting polymers, noncovalent interactions between aromatic building blocks have been mastered by biological systems to elaborate complex machineries such as light-harvesting complexes. Inspired by nature, the last few decades have witnessed tremendous efforts focused on manipulating the structure−function properties of noncovalent assemblies built from stacks of π-conjugated chromophores, a class of materials also named supramolecular polymers.[6−9] The spatial proximity between neighboring units in these noncovalent assemblies promotes interaction of π-electrons leading to the emergence of redox and photophysical properties not achievable by individualized molecular constructs.[10−16] Recent studies focused on investigating the potentiometric properties of supramolecular polymers have highlighted the extent to which structures dictate the functions of noncovalent assemblies.[17−20] In this regard, the conformation of molecular building blocks is a well-known structural parameter that regulates the functions of noncovalent assemblies, where Ångstrom-level displacements suffice to profoundly modify the electronic coupling between neighboring units.[21−24]

Similar to supramolecular polymers, noncovalent interactions among π-conjugated units embedded in the flexible backbones of oligomer scaffolds can be exploited to tune the electronic properties of nanoscale objects.[25−29] This principle

Received: March 12, 2021
Revised: April 16, 2021
Published: May 7, 2021

has been used to engineer, for example, foldamers whose optical functions are regulated by the structural properties of the flexible chains linking the more rigid, redox-active units.[30−32] Solvent polarity and temperature are the two primary experimental handles used to parameterize noncovalent interactions between the π-conjugated units. Seminal work by Iverson and others has shown the emergence of photophysical properties unique to folding states in oligomers built from naphthalene diimide (NDI) electron-acceptor and pyrene electron donor units.[33−35] In contrast, only a few studies have explored the extent to which chemical linkages modulate the redox properties of flexible oligomers.[36] Because flexible repeating units offer a synthetic handle to modulate the electronic interaction of the more rigid π-conjugated segments, they can be leveraged to tune the electrochemical potentials at which electrons and holes are injected into frontier molecular orbitals. While noncovalent interactions between radical π−anions and π−cations have been reported for molecular chromophores,[37−39] the spectroscopic and electron spin properties of p- and n-doped oligomers remain enigmatic. Yet, the molecular engineering of synthetic oligomers whose structure−function properties can be dynamically regulated by the consumption of chemical fuels, such as sacrificial electron donors and acceptors, paves the way to engineer responsive materials that can function far from equilibrium.[40−43]

The electron-acceptor naphthalene diimide has emerged as an appealing building block to devise nanoscale objects equipped with redox-responsive capabilities.[44−47] The synthetic versatility combined with the tunable potentiometric properties of these redox-active units has bolstered the pioneering of supramolecular architectures relevant to solar energy capture and conversion,[48−51] anion sensing,[52−54] and organic electronics.[55−58] Reduced NDI units undergo radical π−anion interactions that give rise to specific absorptive features in the NIR spectral window.[59−61] While this class of noncovalent interactions, specific to reduced NDI units, has mostly been interrogated in organic solvents, only a handful of studies have investigated the interactions of reduced NDI units in aqueous media. Consequently, the extent to which n-doping NDI units can be exploited to tune the electronic functions of water-soluble nanoscale objects is still an open question.

Herein, we present the synthesis and characterization of the two water-soluble **(NDI-Triazo)$_5$** and **(NDI-Am)$_5$** oligomers shown in Scheme 1 that comprise redox-active NDI units and flexible oligoethylene linkers. The two oligomers differ in their linkage topology between the NDI cores where electron-rich triazole moieties are part of the chain scaffold in **(NDI-Triazo)$_5$**. In contrast, the **(NDI-Am)$_5$** oligomer is constructed by direct attachment of its redox units and the ethylene oxide linkers. These two oligomers feature ammonium functionalities that render them water-soluble. Cyclic voltammetry experiments in solution reveal that the linkage topology plays a critical role in dictating the electronic properties of the oligomers where the first reduction potential of **(NDI-Am)$_5$** is stabilized by more than 200 mV as compared to that recorded for **(NDI-Triazo)$_5$**. Exploiting reductive titrations and spectroelectrochemistry, we demonstrate that the n-doped oligomers are characterized by two discrete spectroscopic states, the origin of which is intimately related to the level of n-doping of the oligomer scaffolds. Electron spin resonance spectroscopy further identifies the existence of localized and delocalized electron spin densities, which are shown to be dependent on the oxidation potentials of the sacrificial electron donors used to inject negative charge carriers in the oligomer scaffolds. This study not only provides an in-depth analysis of the spectroscopic and potentiometric properties of neutral and n-doped water-soluble NDI oligomers but also delivers new insights to parameterize electron spin properties in solvated nanoscale objects.

Scheme 1. Synthetic Pathways to Produce the NDI Oligomers (NDI-Triazo)$_5$ and (NDI-Am)$_5$, and the Control Monomers NDI-C≡CH and NDI-C$_2$OH

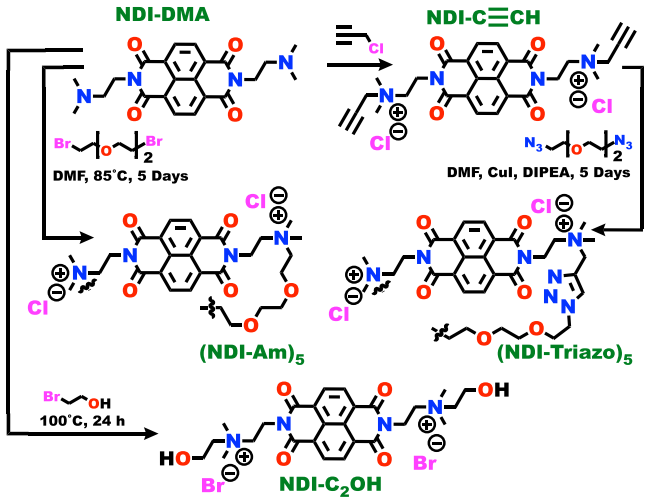

2. METHODS

2.1. Synthesis and Characterization. Scheme 1 summarizes the steps required to synthesize the NDI-derived oligomers and their corresponding monomers. Please refer to the Supporting Information for detailed procedures and spectra.

2.2. X-ray Photoelectron Spectroscopy (XPS) Characterization. The XPS measurements were carried out at the Chapel Hill Analytical and Nanofabrication Laboratory (CHANL) at the University of North Carolina, Chapel Hill. The data were recorded on a Kratos Axis Ultra DLD system with a monochromatic Al Kα source and a base pressure of ca. 6×10^{-9} torr. Survey and high-resolution scans were obtained at pass energies of 80 and 20 eV, respectively. A charge neutralizer was used for charge compensation, and all data were corrected to the C 1s peak at 284.6 eV of binding energy. The signals arising from different elements were deconvoluted (peak fitting) using a Voigt function (30% Lorentzian and 70% Gaussian).

2.3. Gel Permeation Chromatography. The chromatograms shown in Figure 1A,B chronicle the retention times of **(NDI-Triazo)$_5$** and **(NDI-Am)$_5$** oligomers suspended in H_2O/CH_3CN (1:1, v/v) and 0.1 M $NaNO_3$ buffer solutions. The elution profile was best-fitted using one Gaussian function with the peak centered at 23.2 min in the case of **(NDI-Am)$_5$** and 22.9 min in the case of **(NDI-Triazo)$_5$**. The stationary phase Sephacryl S-200 allows the separation of globular proteins and linear dextran polymers. The gel permeation chromatography (GPC) column was calibrated using polystyrene sulfonate as the standard. The choice of this standard was solely based on the solvent buffer condition required to elute the NDI oligomers, namely, **(NDI-Triazo)$_5$** and **(NDI-Am)$_5$**, on the S-200 stationary phase. Using the calibration curve developed from the elution of the polystyrene sulfonate

https://doi.org/10.1021/acs.jpcc.1c02239
J. Phys. Chem. C 2021, 125, 10526−10538

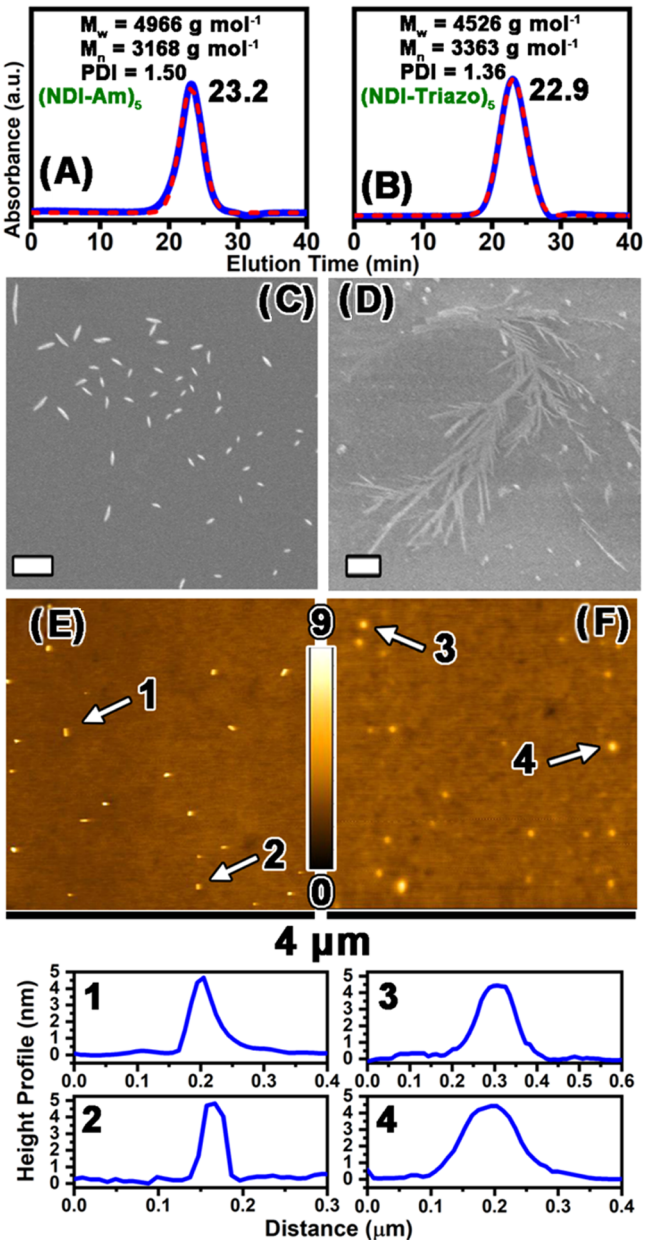

Figure 1. (A, B) Gel permeation chromatograms recorded for the **(NDI-Am)$_5$** (A) and **(NDI-Triazo)$_5$** (B) oligomers. The weight average molecular weight (M_w) and the number average molecular weight (M_n) have been calculated using the calibration curve shown in Section 4 of the Supporting Information. Polydispersity index (PDI) = M_w/M_n. (C, D) Scanning electron microscopy images acquired for the **(NDI-Am)$_5$** (C) and **(NDI-Triazo)$_5$** (D) oligomers drop-cast on the silicon substrate. Scale bars = 1 μm. (E, F) Topographic intermittent contact mode atomic force microscopy (AFM) images of the **(NDI-Am)$_5$** (E) and **(NDI-Triazo)$_5$** (F) oligomers and the associated height profile measurements (1−4).

standard (Figure S4), the weight average molecular weight (M_w), the number average molecular weight (M_n), and the polydispersity index have been calculated for the **(NDI-Am)$_5$** and **(NDI-Triazo)$_5$** oligomers and are tabulated in Figure 1 in the main text.

2.4. Atomic Force Microscopy. The tapping mode AFM images were recorded using a Digital Instruments Dimension 3100 microscope (located at the Dr. John T. Macdonald Foundation BioNIUM Institute in the University of Miami). The microscope was operated with a "Nanoscope 6" controller. The AFM images were collected under air at rt using tapping mode silicon tips (n-type, tip radius < 10 nm, f = 43−81 kHz, k = 0.6−3.7 N/m) obtained from AppNano (FORTA-10). The typical scan rate was 0.8 Hz. The data were analyzed using Gwyddion software (version 2.51). The AFM images were recorded for the two oligomers, namely, **(NDI-Triazo)$_5$** and **(NDI-Am)$_5$**, to analyze their solid-state morphologies. Notably, the sample in each case was prepared by drop-casting the aqueous solution of the oligomer onto Si surfaces at room temperature followed by drying under ambient conditions. The AFM images were recorded on an Agilent 5120 microscope using silicon tips (purchased from AppNano). The microscopic data were analyzed using Gwyddion software to obtain the height profiles associated with the nanoparticles. The representative AFM images pertinent to height profile data for the NDI oligomers are shown below.

2.5. Electrochemical Measurements. The electrochemical measurements were carried out via cyclic voltammetry (CV) using a PARSTAT 3000A potentiostat (Ametek Scientific Instruments). For solution-state electrochemical studies, the cyclic voltammograms were recorded for the aqueous solutions (concentration = 500 μM) of the monomeric (i.e., **NDI-OH** and **NDI-C≡CH**) and oligomeric NDI-based systems (i.e., **(NDI-Triazo)$_5$** and **(NDI-Am)$_5$**) using a glassy carbon working electrode (electroactive surface area = 0.071 cm^2), a platinum counter electrode, a Ag/AgCl (3 M NaCl) reference electrode, and sodium chloride (0.025 M) as the supporting electrolyte under an Ar gas atmosphere at rt. All potentials are reported against SCE using ferrocenecarboxylic acid as internal references (Fc/Fc$^+$ = 0.45 V vs SCE).

2.6. Reductive Titrations. Please refer to Section 8 of the Supporting Information for detailed procedures used to chemically probe the formation of radical π−anions.

2.7. Spectroelectrochemistry Experiments. The spectroelectrochemistry experiments were carried out using a PARSTAT 3000A potentiostat (Ametek Scientific Instruments) and a Cary 5000 UV−vis−NIR spectrophotometer. In a typical experiment, a solution (concentration = 500 μM) of the NDI system in D_2O was gently degassed in a 1.7 mm modified quartz cell. Subsequently, the cell was equipped with a Au honeycomb electrode (that serves as both the working and counter electrodes) and a reference electrode (Ag/AgCl, 3 M NaCl). An initial absorption spectrum was taken as the control, followed by the application of a potential at 0.0 V and the collection of a second absorption spectrum. All potentials were equilibrated for about 10 min or until the applied current plateaued to the smallest possible current (for example, usually lower than −200 μA). All of the experiments were conducted under a gentle flow of Ar to prevent oxygen and water contamination. Subsequently, the ground-state electronic absorption spectrum of the NDI solution was recorded with a gradual increase (i.e., more negative) at the intervals of 50 mV in the cathodic reduction potentials until achievement of the end point of the experiment. It should be noted that by using the ionic nature of the ammonium side chains as part of the NDI systems as leverage, addition of any supporting electrolyte was deemed unnecessary to perform these measurements.

2.8. Electron Paramagnetic Resonance Spectroscopy. All measurements were carried out in D_2O, with the addition of reducing agents under an atmosphere of Ar(g) using

https://doi.org/10.1021/acs.jpcc.1c02239
J. Phys. Chem. C 2021, 125, 10526−10538

previously degassed aqueous (D_2O) solutions. Samples were transferred to torch-sealed quartz capillaries and were subsequently inserted in quartz electron paramagnetic resonance (EPR) tubes (purchased from Wilmad-Labglass). Please note that minimal to no H/D exchange is expected as indicated by ^{1}H NMR. Unless otherwise specified, experiments were performed at room temperature. The magnetic field was centered at 3430 G with a sweep width of 40 G and a sweep time of 2.62 s. The power attenuation was set to 15 dB, with a modulation amplitude of 0.2 G. The data shown in Figures 7 and S17 are the result of 30 scans. Procedures regarding the simulated EPR spectra are detailed in Section 10 of the Supporting Information.

2.9. Density Functional Theory (DFT) and Time-Dependent (TD)-DFT Calculation. Structure optimizations and time-dependent (TD) calculations were performed using density functional theory (DFT) in the Gaussian 09.D01 software package. All calculations were conducted using the truncated molecular structure shown in Figure S18, where the pendant ammonium side chains have been replaced by a methyl substituent. The energy minimization of the monomer building block, dimer, and trimer stack models has been performed using the optimized long-range corrected hybrid density functional ωB97X-D to account for noncovalent interactions between the building blocks. All calculations were conducted using Dunning's correlation consistent double zeta basis set (cc-pvdz). For calculation of the vertical excitation energies in water solvent, a polarized continuum solvation model (SCRF = IEF PCM) with water as the solvent was used.

3. RESULTS AND DISCUSSION

Quaternization of the NDI precursor **NDI-DMA** shown in Scheme 1 provides synthetic access to the **(NDI-Triazo)$_5$** and **(NDI-Am)$_5$** oligomers. While "click" chemistry between the precursor **NDI-C≡CH** and the $N_3(EO)_2N_3$ side chains delivers **(NDI-Triazo)$_5$**, direct functionalization of **NDI-DMA** with the $Br(EO)_2Br$ linker promotes the formation of **(NDI-Am)$_5$**. As shown in Figure 1A,B, gel permeation chromatography characterization performed using a CH_3CN:H_2O solvent mixture unambiguously confirms the formation of oligomer chains characterized by an average of five repeating units for the **(NDI-Triazo)$_5$** and **(NDI-Am)$_5$** constructs. While we acknowledge that the polydispersity index (PDI) calculated for **(NDI-Triazo)$_5$** and **(NDI-Triazo)$_5$** indicates the existence of a heterogeneous distribution of oligomer lengths, the representative number of repeating units, n=5, has been estimated using the number average molecular weight (M_n). X-ray photoelectron spectroscopy was exploited to gain insight into the atomic compositions of the oligomers. The corresponding spectra are shown in Figures S1−S3 and are discussed in Section 3 of the Supporting Information.

To evaluate how the chemical linkages tethering the NDI units impact the solid-state morphologies of the two water-soluble oligomers, scanning electron microscopy (SEM) images were recorded for the **(NDI-Am)$_5$** and **(NDI-Triazo)$_5$** oligomers and are shown in Figure 1C,D, respectively. Additional images are shown in Figures S7 and S8. These images highlight the formation of hierarchical microscale objects, which differ from their solid-state morphologies. As observed in Figure 1D, the **(NDI-Triazo)$_5$** oligomer engenders the formation of fiberlike objects whose sizes span tens of micrometers. In sharp contrast, the **(NDI-Am)$_5$** oligomer evolves, in the solid state, toward discrete, one-dimensional microscale structures with an associated length of 1 μM or smaller. It is important to note that the solid-state morphologies recorded for these samples originate from a drop-cast solution where a concentration effect is likely to favor the formation of the reported microscale objects. To gather more structural information, atomic force microscopy (AFM) images were collected for the **(NDI-Am)$_5$** and **(NDI-Triazo)$_5$** oligomers and are shown in Figure 1E,F, respectively. Additional images are shown in Figures S5 and S6. Dispersed nanoparticles are easily detected for both oligomers where height profile analyses indicate that the thicknesses of these nanostructures vary between 4 and 5 nm. While the resolution offered by AFM does not allow precise determination of structural information for the oligomers, the observed nanoscale objects may be representative of the precursor units that further morph into the hierarchical materials observed by SEM.

Ground-state electronic absorption spectroscopy experiments performed on the NDI-derived oligomers suggest negligible interaction between oligomer chains but indicate electronic coupling between the NDI units embedded in a single oligomer strand. Figure 2A,B compares the electronic

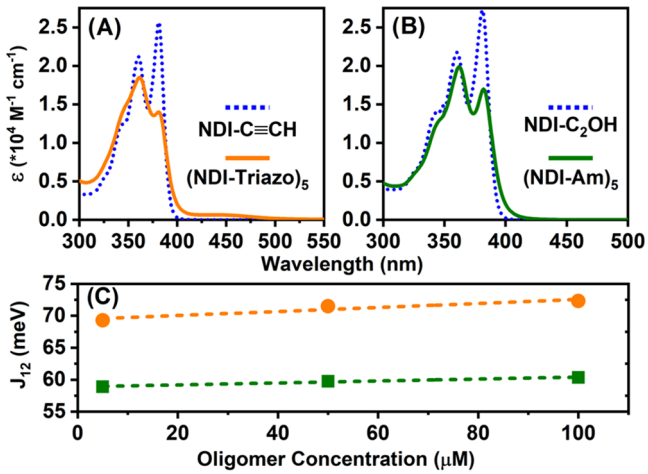

Figure 2. Ground-state electronic absorption spectra recorded in water for the **(NDI-Triazo)$_5$** (A) and **(NDI-Am)$_5$** (B) oligomers. The blue dotted spectra correspond to the control monomers **NDI-C≡CH** and **NDI-C_2OH**. Please note that extinction coefficients for the oligomers are reported per NDI unit considering five repeating units per oligomer chain. (C) Excitonic coupling calculated for the **(NDI-Triazo)$_5$** (orange bullets) and **(NDI-Am)$_5$** (green squares) oligomers, in water, as a function of the oligomer concentration.

absorption spectra (EAS) of the **(NDI-Triazo)$_5$** and **(NDI-Am)$_5$** oligomers to those collected for the NDI monomer controls **NDI-C≡CH** and **NDI-C_2OH**, respectively. Across the concentration range probed (5−100 μM), these two monomers solvated in aqueous medium evidence the spectroscopic hallmarks of individualized units as confirmed by the identical ratio (~1.20) of the 0−0 and 0−1 vibronic transitions centered at 381 and 360 nm, respectively. This finding indicates a lack of electronic interaction between the NDI precursor units. In contrast to this result, the EAS collected for the **(NDI-Triazo)$_5$** and **(NDI-Am)$_5$** oligomers highlight a change of the 0−0 and 0−1 vibronic transition intensities centered at 379 and 362 nm, respectively, that indicate non-negligible degrees of NDI unit interactions. These

https://doi.org/10.1021/acs.jpcc.1c02239
J. Phys. Chem. C 2021, 125, 10526−10538

well-documented spectroscopic attributes accompany the formation of H-like aggregates.[59]

To quantify the degree of electronic interaction between NDI units, the excitonic coupling J_{12} was calculated by exploiting the model developed by Spano and used by us, and others, on rylene-derived aggregates.[20,23,62−64] Figure 2C reports the J_{12} values calculated for the **(NDI-Triazo)$_5$** and **(NDI-Am)$_5$** oligomers as a function of the oligomer concentration. While the excitonic coupling among NDI units in **(NDI-Triazo)$_5$** is modestly higher than that calculated for the **(NDI-Am)$_5$** oligomers, it is interesting to note that the J_{12} values for both oligomers vary only marginally across the concentration range probed (5−100 μM). The fact that the excitonic coupling does not appear to be sensitive to oligomer concentration signals negligible structural perturbation of the oligomer chains. It is well known that the excitonic properties of π-conjugated aggregates are regulated by the conformation of the building blocks where Ångstrom-level displacements regulate the photophysical properties at the assembly level.[22,23] If the photophysical properties of NDI-derived oligomers were originating from interactions between NDI units featured on different oligomer chains (interchain interactions), a more pronounced perturbation of the excitonic coupling would be expected as a function of oligomer concentration. To this end, we posit that the excitonic coupling reported for the NDI-derived oligomers originates from interactions of NDI units within a single oligomer chain (intrachain interactions). Even at a low concentration of oligomers (5 μM), the close spatial proximity of NDI units embedded in a single oligomer chain may promote non-negligible electronic interactions.

Electrochemical experiments unveil the extent to which the chemical structure of the flexible chain units regulates the potentiometric properties of the NDI-derived oligomers. Figure 3 compares the cyclic voltammograms recorded for the **(NDI-Am)$_5$** and **(NDI-Triazo)$_5$** oligomers with those of the control NDI monomers **NDI-C$_2$OH** and **NDI-C≡CH**, respectively. As shown in Figure 3A,C, the two NDI monomers share similar potentiometric properties by evidencing two reversible redox waves at $E^{-/0}$ = −0.352 V and $E^{2-/-}$ = −0.698 V for the solvated **NDI-C$_2$OH** units and $E^{-/0}$ = −0.346 V and $E^{2-/-}$ = −0.673 V for the solvated **NDI-C≡CH** units. The associated anodic and cathodic peaks are shown in Figures S9 and S10 in the Supporting Information, respectively. These waves diagnose the first and second reduction potentials of individualized NDI cores. As expected, the alcohol side chain and ethynyl fragments functionalizing the ammonium groups on **NDI-C$_2$OH** and **NDI-C≡CH**, respectively, do not perturb the electronic properties of the redox-active cores. In sharp contrast, the cyclic voltammograms recorded for the **(NDI-Am)$_5$** and **(NDI-Triazo)$_5$** oligomers, in an aqueous medium, differ from those acquired for the parent NDI monomers, suggesting that the oligomers are equipped with a more complex electronic structure. As shown in Figure 3D, a number of redox waves are observed when swiping toward cathodic potentials for the **(NDI-Triazo)$_5$** oligomers, whereby complicating the potentiometric analysis. To gain a more meaningful insight, we calculated the inflection point characterizing the first cathodic transition ($E^{(i)}$) using the method recently reported by Vullev.[65] This approach allows us to reliably estimate the first reduction potential of the oligomers and compare them to those calculated for the monomers. The **(NDI-Triazo)$_5$** oligomer demonstrates a first reduction potential centered at −0.250 V vs SCE that is anodically

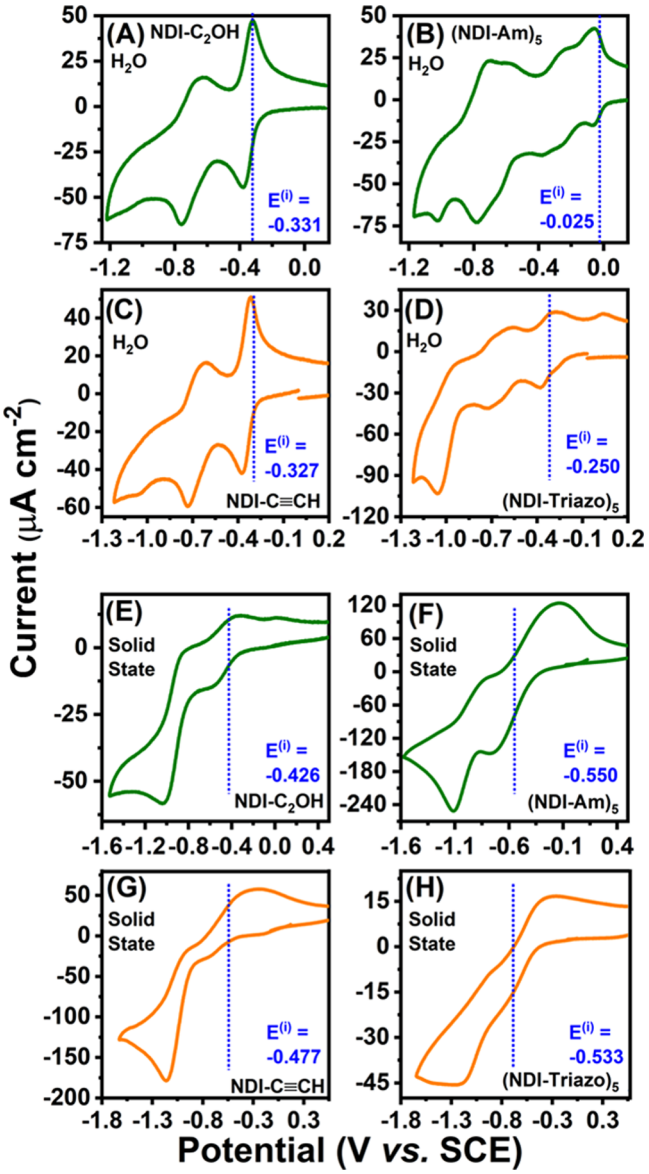

Figure 3. (A−D) Solution-phase cyclic voltammograms of the control monomers **NDI-C$_2$OH** (A) and **NDI-C≡CH** (C) are compared to those recorded for the NDI oligomers **(NDI-Am)$_5$** (B) and **(NDI-Triazo)$_5$** (D). (E−H) Cyclic voltammetry measurements performed on drop-cast control monomers **NDI-C$_2$OH** (E) and **NDI-C≡CH** (G) and the NDI oligomers **(NDI-Am)$_5$** (F) and **(NDI-Triazo)$_5$** (H). Experimental conditions: scan rate = 50 mV s^{-1}, glassy carbon working electrode, and Ag/AgCl reference electrode. Potentials have been converted to SCE using Fc/Fc$^+$ as the internal standard. Please see Section 7 in the Supporting Information for more details regarding the estimation of the first reduction inflection point $E^{(i)}$ and the solvent conditions.

shifted with respect to that assessed for the corresponding NDI monomer ($E^{(i)}$ = −0.327 V vs SCE). A succession of undefined redox waves is observed during the excursion toward a final cathodic potential (−1.20 V vs SCE), indicating that the oligomer possesses a more complex electronic structure than the monomer. However, the fact that electron injection is facilitated by 77 mV for the **(NDI-Triazo)$_5$** oligomer may stem from the close spatial proximity of the NDI units within the oligomer chains that screen the injected negative charge carriers.

https://doi.org/10.1021/acs.jpcc.1c02239
J. Phys. Chem. C 2021, 125, 10526−10538

Similar to the observation made for the **(NDI-Triazo)$_5$** oligomer, the cyclic voltammogram recorded for the **(NDI-Am)$_5$** derivative differs significantly from that collected for the parent monomer **NDI-C$_2$OH** and highlights more complex reduction and back-oxidation processes spanning the cathodic potential window (0 to −1.2 V). This finding is likely to originate from a screening effect caused by the initially reduced NDI units that render further electron injection into the oligomer chain less favorable. A similar observation has been made for NDI-derived rotaxanes.[66] The first reduction potential recorded for the **(NDI-Am)$_5$** oligomer shown in Figure 3B is centered at −0.025 V vs SCE, indicating a significant stabilization of the lowest unoccupied molecular orbitals (LUMOs) as compared to the parent monomer ($E^{-/0}$ = −0.331 V vs SCE). A potential explanation for this observation is that intermolecular charge-transfer states engendered by the close proximity of NDI units in the oligomer scaffold may stabilize the initially injected negative charge carriers to a larger extent. Furthermore, the fact that the first reduction potential of the **(NDI-Am)$_5$** ($E^{-/0}$ = −0.025 V vs SCE) and **(NDI-Triazo)$_8$** oligomers ($E^{-/0}$ = −0.250 V vs SCE) is so markedly different highlights the non-negligible role played by the side chains that link the NDI units in regulating the redox properties of these oligomers. The electron-rich triazole linkage in the **(NDI-Triazo)$_5$** oligomer may interact with the more electron-deficient NDI core, thus destabilizing the first reduction potential of the redox-active chromophore. In contrast, the linkage topology exploited to construct the **(NDI-Am)$_5$** oligomer facilitates the reduction of the NDI cores enabling the engineering of redox-active nanoscale objects that possess low-lying electronic states.

The potentiometric properties reported for the NDI oligomers in the solid state differ markedly from those in solution. Figure 3E−H chronicles the cyclic voltammograms recorded using modified glassy carbon electrodes, on which a solution of the NDI oligomers (Figure 3F,H) and control NDI monomers (Figure 3E,G) has been drop-cast. Similar to solution phase, the solid-state control NDI monomers share similar first reduction potentials as attested by the evaluation of the first inflection potentials shown in Figure 3E,G for the **NDI-C$_2$OH** ($E^{(i)}$ = −0.321 V vs SCE) and **NDI-C≡CH** ($E^{(i)}$ = −0.327 V vs SCE) constructs. However, when compared to the solvated analytes in H_2O (Figure 3A,C), a general destabilization of the first reduction potentials is witnessed and is a consequence of the change of the dielectric constant between the aqueous medium (∼80) and the solid-sate organic matter compositions (∼4). It is interesting to underscore that the **(NDI-Am)$_5$** and **(NDI-Triazo)$_5$** oligomers featuring virtually identical first inflection potentials (centered at −0.550 and −0.533 V, respectively) are modestly destabilized as compared to those measured for the control monomers in the solid state. This observation is in sharp contrast to the potentiometric properties shown in Figure 3A−D for the solvated oligomers and their corresponding monomers. We hypothesize that the stabilization of the first inflection points observed for both solvated oligomers originates from a screening of the n-doped states by neighboring, neutral NDI units. In solution, the degree of freedom of the flexible ethylene oxide chains allows for structural reorganization of the NDI units, enabling the stabilization of the radical π−anions. The reductive titrations along with the spectroelectrochemical and the electron paramagnetic resonance measurements presented below further support this assumption.

Because the **(NDI-Am)$_5$** and **(NDI-Triazo)$_5$** oligomers are equipped with low-lying first reduction potentials, sodium ascorbate (NaAsc) can be exploited to probe the spectroscopic signatures of the n-doped oligomers in an aqueous solvent. This vitamin C derivative is characterized by a reduction potential of −0.290 V vs SCE, therefore representing an ideal titrant to partially reduce the NDI oligomers. The EAS associated with the reductive titration experiments are shown in Figure 4 and reveal absorptive features, in the NIR spectral

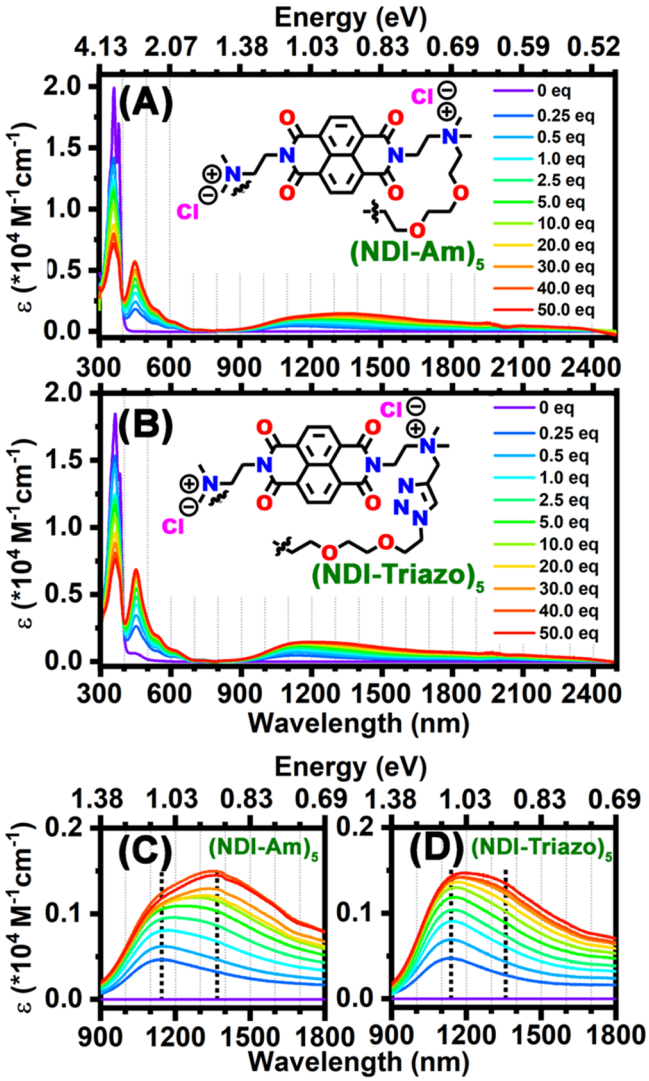

Figure 4. (A, B) Reductive titration spectra recorded for the **(NDI-Am)$_5$** and **(NDI-Triazo)$_5$** oligomers using NaAsc as the sacrificial electron donor. (C, D) Zoom-in of the NIR spectral window of panels (A) and (B). Experimental conditions: $(NDI)_{oligomer}$ = 100 μM, t = 20 °C; argon atmosphere; optical pathlength = 2 mm; and solvent = D_2O. Please note that extinction coefficients for the oligomers are reported per NDI unit considering five repeating units per oligomer chain.

window, diagnostic of NDI π−anion interactions. For both the **(NDI-Am)$_5$** and **(NDI-Triazo)$_5$** oligomers shown in Figure 4A,B, respectively, the addition of NaAsc is accompanied by a decrease in the oscillator strength associated with the exciton spectral features at 360 and 381 nm and a concomitant increase of new transitions centered at 449, 548, and 626 nm. Furthermore, broad absorption bands are unambiguously

https://doi.org/10.1021/acs.jpcc.1c02239
J. Phys. Chem. C 2021, 125, 10526−10538

detected in the 900 to 2500 nm spectral window whose intensities appear to evolve as a function of NaAsc equivalency (0.25−50 equiv). While the addition of a low equivalency of sacrificial electron donor (0.25−0.5 equiv) promotes the formation of an absorptive feature at 1140 nm in both the $(\mathbf{NDI\text{-}Triazo})_5$ and $(\mathbf{NDI\text{-}Am})_5$ oligomers, as seen in Figure 4C,D, it is interesting to note the increase of a new spectroscopic feature appearing as a low-energy shoulder at ∼1360 nm that is more prominent upon reduction of the $(\mathbf{NDI\text{-}Am})_5$ oligomers (Figure 4C) than it is for the $(\mathbf{NDI\text{-}Triazo})_5$ oligomers (Figure 4D). This observation indicates that the structures of the $(\mathbf{NDI\text{-}Am})_5$ oligomers enable the formation of n-doped states that are less favored in the $(\mathbf{NDI\text{-}Triazo})_5$ oligomers, under identical reductive titrant concentrations. Closely related spectroscopic signals have been reported for n-doped π-stacks built from water-soluble NDI monomers and for covalently linked NDI dimers.[59−61,67] In these molecular systems, the spatial proximity of NDI cores enforces intermolecular charge-transfer interactions as well as radical π−anion interactions that lead to nascent electronic states at the origin of the absorption bands observed in the NIR spectral windows. Furthermore, it is interesting to note that reductive titrations of the control monomers using NaAsc do not engender the formation of the spectroscopic features observed for the oligomer analogues as this sacrificial electron donor does not possess the required thermodynamic driving force to n-dope the molecular NDI units. Please refer to Section 8 and Figure S13 in the Supporting Information.

The n-doping of the $(\mathbf{NDI\text{-}Am})_5$ and $(\mathbf{NDI\text{-}Triazo})_5$ oligomers via a sacrificial electron donor that possesses a more negative reduction potential than NaAsc allows a more detailed analysis of the NIR spectral windows and enables us to scrutinize the heterogeneity of molecular interactions of the reduced NDI units as a function of oligomer chains. As chronicled in Figure 5A, the addition of up to 0.5 equiv of sodium hydrosulfide (NaSH, $E^{-/0} \sim -0.55$ V vs SCE) to the $(\mathbf{NDI\text{-}Triazo})_5$ oligomers engenders spectral modifications mimicking those reported upon the addition of 50 equiv of NaAsc as the sacrificial electron donor. No drastic spectral changes are detected after the addition of 3 equiv of NaSH, signaling saturation of the oligomer chain doping under these experimental conditions. As shown in Figure 5C, the spectral decomposition of the NIR transition (0.5 equiv of NaSH) using two Gaussian functions unveils two distinct bands centered at 1142 nm (1.085 eV) and 1399 nm (0.886 eV). Interestingly, increasing the number of equivalents of NaSH (3 equiv, saturation conditions) is associated with noticeable perturbation of the NIR transitions, as seen in Figure 5D. Most notably, an increase in intensity of the low-energy band initially centered at 1399 nm (0.5 equiv of NaSH) along with its bathochromic shift to 1481 nm (3 equiv of NaSH) is observed.

Figure 5B highlights the EAS collected during the reductive titration of the $(\mathbf{NDI\text{-}Am})_5$ oligomers and electronic spectral properties that differ, to some extent, from those reported for the $(\mathbf{NDI\text{-}Triazo})_5$ oligomers. At a low equivalency of reductant (0.25 equiv of NaSH), broad absorptive features spanning the 825 to 2500 nm spectral window are detected. This is in marked contrast to the more resolved band observed during the titration of the $(\mathbf{NDI\text{-}Triazo})_5$ oligomers at identical NaSH equivalency (please refer to Figure 5A). Increasing the sacrificial electron donor to 0.5 equiv promotes the increase of a distinct absorptive band centered at 1476 nm, which is associated with a blue shoulder at 1170 nm. The

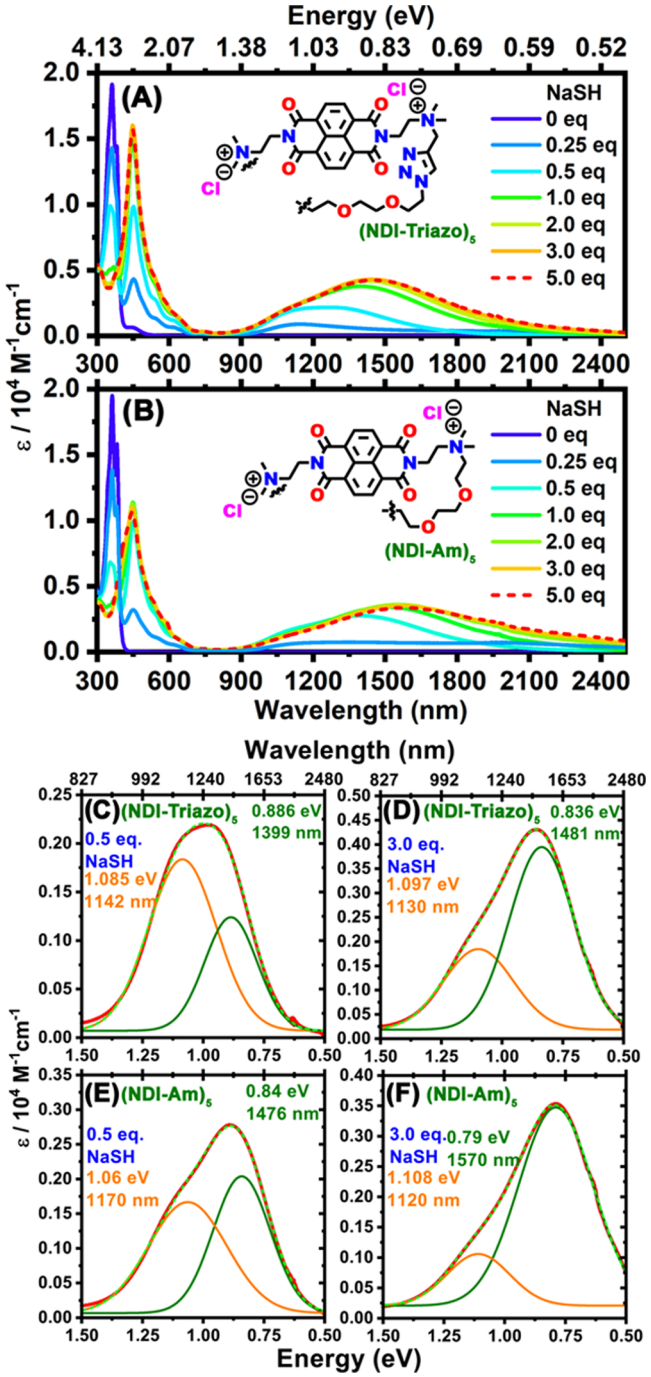

Figure 5. (A, B) Reductive titration spectra recorded for the $(\mathbf{NDI\text{-}Am})_5$ and $(\mathbf{NDI\text{-}Triazo})_5$ oligomers when using NaSH as the sacrificial electron donor. (C−F) Deconvolution of the NIR spectral window as a function of NaSH equivalency. Experimental conditions: $(\mathrm{NDI})_{\mathrm{oligomer}}$ = 100 μM, t = 20 °C; argon atmosphere; optical pathlength = 2 mm; and solvent = D_2O. Please note that extinction coefficients for the oligomers are reported per NDI unit considering five repeating units per oligomer chain.

deconvoluted spectra are chronicled in Figure 5E. Further addition of up to 3 equiv of NaSH is accompanied by the increase of absorptivity of the NIR absorption band initially centered at 1476 nm and an apparent red shift to 1570 nm ($\Delta\lambda$ = 94 nm, ΔE = 46 meV). No substantial spectroscopic perturbations are witnessed when increasing the concentration of the sacrificial electron donor to 5 equiv, thus confirming

https://doi.org/10.1021/acs.jpcc.1c02239
J. Phys. Chem. C 2021, 125, 10526−10538

saturation of the NDI oligomer. Under identical experimental conditions, it is interesting to note that the energy of the low-energy NIR transition associated with the n-doped $(\mathbf{NDI\text{-}Am})_5$ oligomers (λ_{abs} = 1570 nm, E_{abs} = 0.790 eV) is stabilized by 46 meV when compared to that evidenced during the titration of $(\mathbf{NDI\text{-}Triazo})_5$ oligomers (λ_{abs} = 1481 nm, E_{abs} = 0.836 eV). This observation suggests that the linkage topology in $(\mathbf{NDI\text{-}Am})_5$ oligomers may enforce a higher degree of reduced NDI interactions when compared to that supported by the $(\mathbf{NDI\text{-}Triazo})_5$ oligomer. This hypothesis is based on the seminal work by Miller et al. who have reported similar NIR red shifts for n-doped π-stacks built from NDI units flanked with various side-chain functionalities.[67]

The reductive titration experiments conducted on the control monomers **NDI-C$_2$OH** and **NDI-C≡CH** using NaSH as the sacrificial electron donor are shown in Figure S14. In contrast to the oligomer analogues, the addition of NaSH (up to 10 equiv) to a solution of the NDI monomers does not promote the formation of the broad NIR band where only perturbation of the visible part of the spectral window is observed. These experimental conditions do not enable the formation of NDI radical π−anion interactions that are unique to the oligomer constructs. This finding further highlights the advantage of embedding NDI redox units in an oligomer scaffold to engineer redox-responsive nanoscale objects.

To glean more insights into the origin of the NIR transitions observed during the reductive titrations of the $(\mathbf{NDI\text{-}Am})_5$ and $(\mathbf{NDI\text{-}Triazo})_5$ oligomers, time-dependent density functional theory (TD-DFT) calculations were performed on singly reduced NDI dimer ($[NDI]_2^{\bullet-}$) and trimer ($[NDI]_3^{\bullet-}$) models. Please refer to Section 11 in the Supporting Information for more details. As shown in Table 1, the n-doped dimer and trimer models are characterized by vertical, low-energy NIR transitions centered at 1658 nm (0.7478 eV) and 1374 nm (0.9021 eV), respectively. These calculated vertical transitions are dominated by HOMOα → LUMOα for $[NDI]_2^{\bullet-}$, and HOMOα → LUMOα and HOMOα → LUMOα+1 for $[NDI]_3^{\bullet-}$; the relevant molecular orbitals are depicted in Figure 6. These data indicate that the low-energy transitions observed for the dimer and trimer models have significant intermolecular charge-transfer characters as indicated by the redistribution of the electronic density from one NDI unit to another. The fact that the low-energy transition computed for the trimer stack shifts toward higher energy, as compared with that calculated for the dimer, may originate from the close proximity of two neighboring π-conjugated NDIs. In addition, it is interesting to note that the lowest-energy transition computed for the monomer NDI radical π−anion is centered at 624 nm (1.9867 eV), in contrast to the NIR vertical wavelengths computed for the dimer and trimer NDI stack models.

Table 1. Vertical Wavelength (λ_{abs}), Oscillator Strengths (f), and Dominant Orbital Characters for the Low-Energy Transition Computed Using TD-DFT Methods for the Singly Reduced NDI Monomer NDI ($[NDI]^{\bullet-}$), Dimer ($[NDI]_2^{\bullet-}$), and Trimer ($[NDI]_3^{\bullet-}$) Models

	λ_{abs} (nm/eV)	f	dominant orbital characters
$[NDI]^{\bullet-}$	624/1.987	0.0615	Hα → Lα (96 %)
$[NDI]_2^{\bullet-}$	1658/0.748	0.0659	Hα → Lα (98 %)
$[NDI]_3^{\bullet-}$	1374/0.902	0.0654	Hα → Lα (45 %)
			Hα → L + 1α (53 %)

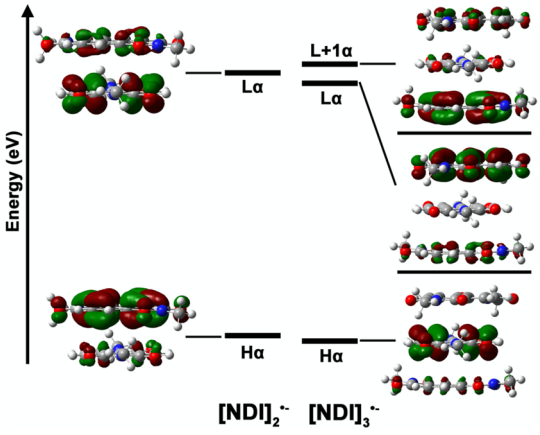

Figure 6. Frontier molecular orbitals of the singly reduced NDI dimer ($[NDI]_2^{\bullet-}$) and NDI trimer ($[NDI]_3^{\bullet-}$) stack models calculated using DFT at the ωB97X-D level of theory. Basis set = cc-pvdz, solvent = water. Please refer to Section 11 in the Supporting Information for more details.

The TD-DFT calculations provide supporting evidence that the experimental NIR transitions observed during the titrations of the oligomers are diagnostic of noncovalent interactions involving NDI π−anions. However, some limitations of our current model have to be acknowledged. More complex electronic processes are likely to arise in the n-doped NDI oligomers due to the number of repeating units (∼5) in addition to the structural degrees of freedoms that our current model fails to capture. Furthermore, the TD-DFT calculations have been performed on singly reduced dimer and trimer NDI models. Higher levels of n-doping of the oligomer chains enable the formation of new spectroscopic states as diagnosed during the reductive titration experiments that exploit NaSH as the sacrificial electron donor.

Together, the electrochemical experiments, the reductive titrations performed on the $(\mathbf{NDI\text{-}Triazo})_5$ and $(\mathbf{NDI\text{-}Am})_5$ oligomers, and the TD-DFT calculations of the model dimer and trimer NDI stacks indicate the existence of complex n-doped states whose formations are contingent not only on NDI interactions but also on the concentration of electrons per oligomer chain. At low equivalencies of NaAsc (0.25 equiv), the NDI oligomer chains are partially reduced. Consequently, the spectroscopic features centered at 1140 nm may originate from intermolecular charge-transfer interactions between a reduced NDI unit and a neutral NDI unit. This hypothesis is supported by TD-DFT. It is interesting to note that this spectroscopic feature is also observed, for both oligomers, during the reductive titrations that exploit a low equivalency of NaSH (0.5 equiv) (please refer to Figure 5). Increasing the concentration of NaAsc enforces a higher level of n-doping of the oligomer chain, a process characterized by the increase of the NIR absorption band centered at 1360 nm, which is more prominent in the $(\mathbf{NDI\text{-}Am})_5$ oligomers (Figure 4). Because the redox potential of NaAsc does not provide sufficient driving force to further reduce the oligomer chain, exploitation of the stronger reductant NaSH provides a means to enforce a higher level of n-doping. As the concentration of NaSH increases from 0.5 to 3.0 equiv, the concomitant increase and red shift of the NIR band initially centered at 1399 and 1476 nm for the $(\mathbf{NDI\text{-}Triazo})_5$ and $(\mathbf{NDI\text{-}Am})_5$ oligomers, respectively, diagnose the emergence of spectroscopic states not accessible using NaAsc as a reductant.

https://doi.org/10.1021/acs.jpcc.1c02239
J. Phys. Chem. C 2021, 125, 10526−10538

To confirm the absorptive features characterizing the n-doped NDI oligomers and further investigate the electrochemical potentials required to generate these spectroscopic signatures, spectroelectrochemistry experiments were performed on the **(NDI-Triazo)$_5$** and **(NDI-Am)$_5$** derivatives; the respective spectra are shown in Figure 7. For the **(NDI-Triazo)$_5$** oligomer shown in Figure 7A,B, increasing the cathodic potentials from 0 to −0.30 V vs SCE is associated with the increase of a broad NIR band. The deconvoluted spectra shown in Figure S15 reveal two distinct bands centered at 1130 nm (1.09 eV) and 1411 nm (0.87 eV). These NIR absorptive features mimic those generated using NaAsc (5 equiv) or a low equivalency of NaSH (0.25 equiv). Further excursion from −0.30 to −0.60 V vs SCE is associated with the increase in intensity of the lowest-energy transitions centered at 1411 nm. Increasing the cathodic potential to −0.9 V results in the loss of the spectroscopic signals in the NIR spectral window and the emergence of transitions centered at 581, 540, and 500 nm. These absorptive features signal the formation of the NDI dianion derivative. As compared to the reductive titrations that exploit the sacrificial electron donor NaSH, it is interesting to note that no apparent red shift of the low-energy NIR transitions centered at 1411 nm is observed. Because the NDI oligomers are polyelectrolytes, no supporting electrolyte is used during the spectroelectrochemistry experiments, allowing us to monitor the spectroscopic signatures of the negative charge carriers in the absence of additional salts. In this regard, the apparent red shift of the NIR transitions exclusively observed during the reductive titration experiments may be attributed to the stabilization of the negative charge carriers by countercations. In addition, as the concentration of the ionic titrant increases, so does the ionic strength of the solution, which may induce conformational changes of the oligomer chains.

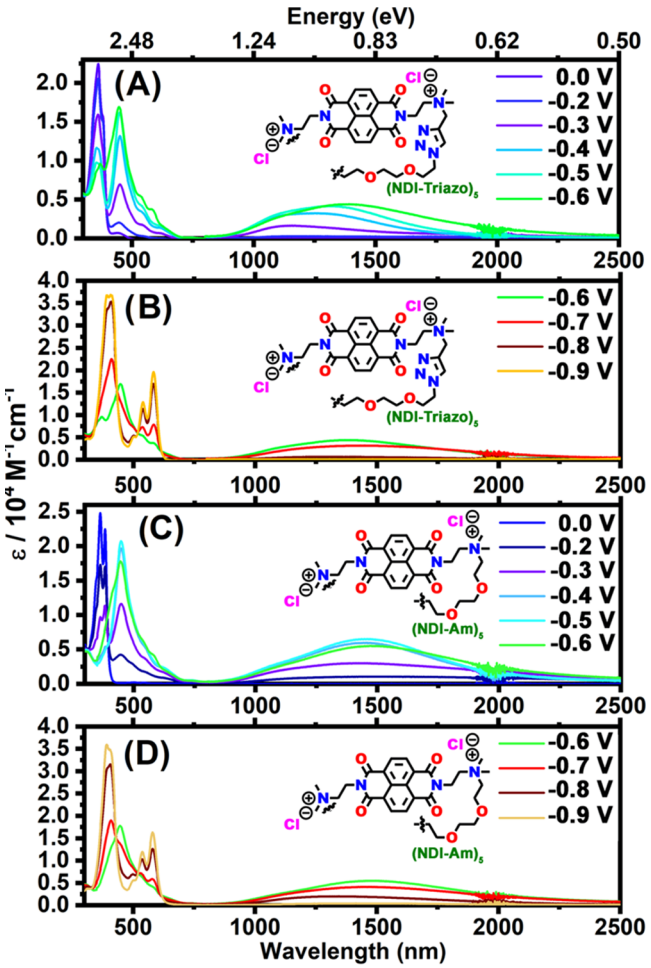

Figure 7. Electrochemically generated spectra in deuterated water solvents that chronicle the change of spectroscopic properties recorded for the **(NDI-Triazo)$_5$** (A,B) and **(NDI-Am)$_5$** (C,D) oligomers. Experimental conditions: $(NDI)_{oligomer}$ = 100 μM; argon atmosphere; optical pathlength = 1 mm; gold-mesh working electrode; room temperature (20 °C); and platinum counter electrode. All potentials are reported against SCE. Please note that extinction coefficients for the oligomers are reported per NDI unit considering five repeating units per oligomer chain.

In Figure 7C,D, the spectroelectrochemical measurements performed on the **(NDI-Am)$_5$** oligomer highlight spectroscopic features that share some resemblance to those elucidated during the reductive titrations. Specifically, a cathodic potential of −0.20 V vs SCE enforces the formation of a broad NIR transition mimicking that generated using 0.25 equiv of NaAsc. As the cathodic potential is increased from −0.15 to −0.55 V vs SCE, a continuous increase of the NIR spectroscopic features initially centered at 1080 nm (1.147 eV) and 1461 nm (0.848 eV) is witnessed. The deconvoluted spectra are shown in Figure S16. This analysis reveals a modest red shift of the low-energy NIR band initially centered at 0.848 eV ($\Delta\lambda$ = 46 nm, ΔE = 26 meV) as compared to that observed during the reductive titration of the **(NDI-Am)$_5$** oligomers when adding up to 3 equiv of NaSH ($\Delta\lambda$ = 94 nm, ΔE = 50 meV). Similar to the observation made for the **(NDI-Triazo)$_5$** derivative, this finding may be attributed to the decrease in screening of the injected negative charges by sodium cations during the spectroelectrochemical experiments where the supporting electrolyte is absent. To conclude the spectroelectrochemical experiments, the cathodic potential is increased to −0.9 V vs SCE. As shown in Figure 7D, the spectroscopic signatures of the doubly reduced NDI units are unambiguously detected at this potential, as observed by the increase of new absorptive features centered at 579, 535, and 496 nm.

The reductive titrations and spectroelectrochemical experiments confirm the formation of two distinguishable n-doped spectroscopic states. While the high-energy NIR absorptive feature observed at ∼1140 nm is characteristic of a low doping level of the NDI oligomer chains, the emergence of the low-energy transition observed in the presence of increasing potentials or higher concentrations of sacrificial electron donors is diagnostic of a higher level of n-doping. It is interesting to note that even at elevated concentrations of sacrificial electron donor, the high-energy NIR absorptive feature (∼1140 nm) is present for both oligomers, albeit the low-energy NIR transition is the most intense under this condition.

To gain further insight into the electron spin properties of the n-doped states generated in the presence of NaAsc and NaSH as sacrificial electron donors, we employed electron paramagnetic resonance (EPR) spectroscopy. The room-temperature X-band EPR spectrum of the parent monomer **NDI-C$_2$OH** in the presence of 50 equiv of NaAsc is shown in Figure 8A (black curve). The lack of EPR-active species confirms that, even at 50 equiv, NaAsc lacks the necessary driving force to reduce the molecularly dissolved monomers. In contrast, the EPR signal recorded for the NDI monomer in the

https://doi.org/10.1021/acs.jpcc.1c02239
J. Phys. Chem. C 2021, 125, 10526−10538

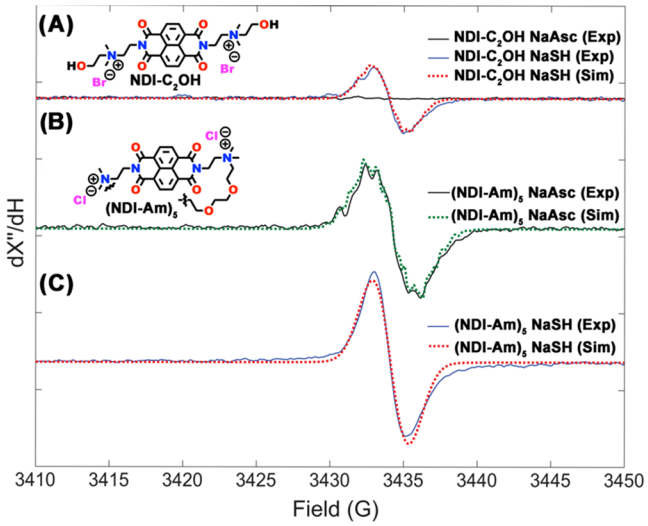

Figure 8. Room-temperature, X-band EPR spectra of **NDI-C$_2$OH** and **(NDI-Am)$_5$** in the presence of either NaAsc or NaSH as the sacrificial reductant. (A) Overlay of **NDI-C$_2$OH** in the presence of NaAsc, experimental spectrum (black, solid) with **NDI-C$_2$OH** in the presence of NaSH, experimental (blue, solid), and simulation (red, dashed). (B) Experimental (black, solid) and simulated (green, dashed) spectra of **(NDI-Am)$_5$** in the presence of 50 equiv of NaAsc. (C) Experimental (blue, solid) and simulated (red, dashed) spectra of **(NDI-Am)$_5$** in the presence of 5 equiv of NaSH. All experimental spectra were recorded under nonsaturating conditions: 9.63 GHz microwave frequency, 15 dB power attenuation, and 0.2 G modulation amplitude.

presence of NaSH as a sacrificial electron donor (Figure 8A, solid blue line) reveals a characteristic $S = 1/2$ signal with discernible hyperfine features. The experimental spectrum was simulated using the EasySpin[68] open source MatLab program and an $S = 1/2$ spin Hamiltonian (Figure 8A, red dashed line) that included nuclear hyperfine coupling terms for 14 nuclei: two $I = 1$ ^{14}N nuclei and three sets of four equivalent $I = 1/2$ ^{1}H nuclei: $(^{14}N) = 1.05(5)$, $A(^{1}H) = 1.35(7)$, $A(^{1}H) = 1.63(5)$, $A(^{1}H) = 2.08(7)$ MHz. All simulations were calculated using an isotropic g-value of 2.0038(2). In contrast, however, EPR data recorded for the **(NDI-Am)$_5$** oligomers in the presence of 50 equiv of NaAsc revealed the presence of sharp hyperfine features spread across the isotropic curve. The simulated spectrum shown in Figure 8B (green dashed curve) was generated using a spin Hamiltonian with hyperfine coupling between the unpaired electron and ^{14}N/^{1}H nuclei of the NDI unit. Importantly, this result is consistent with the depiction of **(NDI-Am)$_5$** in the presence of NaAsc, where the unpaired electron spin is principally located on a single NDI unit. The isotropic hyperfine coupling constants for the NDI nuclei of the NDI unit, in units of MHz, are $A(^{14}N) = 1.40(5)$, $A(^{1}H) = 1.78(5)$, and $A(^{1}H) = 2.60(10)$. Notably, the EPR spectrum of the **(NDI-Am)$_5$** oligomers n-doped with 5 equiv of NaSH is characterized by an apparent lack of discernible hyperfine coupling. This observation is most consistent with a description where the unpaired spin density is delocalized over two NDI repeating units in the **(NDI-Am)$_5$** oligomer chain. Simulation of the experimental spectrum is successfully achieved by including twice the number of nuclei with hyperfine coupling constants of $A(^{14}N) = 0.50(10)$, $A(^{1}H) = 0.72(10)$, $A(^{1}H) = 1.05(20)$, and $A(^{1}H) = 1.09(20)$ MHz.

The fact that the electron spin properties of the n-doped **(NDI-Am)$_5$** oligomer are dependent upon the nature of the sacrificial electron donors confirms the existence of disparate electronic states also observed by ground-state electronic absorption spectroscopy. In particular, the addition of 50 equiv of NaAsc results in the unpaired electron density being localized on one NDI unit and corresponds to the lowest-energy states accessible in the partially n-doped **(NDI-Am)$_5$** oligomer. In contrast, the stronger reducing titrant, NaSH, enables the injection of electrons into higher-lying electronic states not accessible by NaAsc, whereby delocalizing the electron wave function over two NDI repeating units. One can rationalize this observation by assuming that the NDI units must lie in close spatial proximity to one another.

Since it is unlikely that all of the NDI units comprised in an **(NDI-Am)$_5$** oligomer chain share identical solvation environments, our current hypothesis relies on the fact that the low-lying n-doped states formed using NaAsc as the sacrificial electron donor may correspond to reduced NDI units having a higher degree of solvent interactions. Under this condition, weaker NDI π−anion interactions may limit the unpaired electron spin delocalization. Although this hypothesis remains to be tested, variability in solvation spheres may explain the observed differences in both the EAS and EPR measurements, which are likely attributed to the position of the NDI units in the oligomer chains.

To probe if the n-doped oligomer states created when using NaAsc as the sacrificial electron donor evolve as a function of time, a solution of the **(NDI-Am)$_5$** oligomer under saturated conditions (50 equiv of NaAsc) was left to age over 20 days under an argon atmosphere. The corresponding EPR spectrum is shown in Figure S17. Comparison of the EPR signal of the freshly n-doped ($t = 0$ days) **(NDI-Am)$_5$** oligomer with that of the aged ($t = 20$ days) sample reveals a loss of discernible hyperfine features. It is interesting to note that the simulation of the experimental spectrum of the aged ($t = 20$ days) **(NDI-Am)$_5$** sample can be achieved using a Hamiltonian containing twice the total number of nuclei, with hyperfine coupling values that are approximately half of those used in the $t = 0$ simulation. This finding suggests that, over time, the electron spin becomes delocalized over two NDI repeating units. This is in contrast to the localized electron spin properties highlighted previously for the freshly n-doped sample ($t = 0$ days) and instead is more reminiscent of the electron spin properties of the **(NDI-Am)$_5$** oligomer in the presence of NaSH. The evolution of the electron spin properties as a function of time may originate from two phenomena. First, slow structural reorganization of the NDI oligomer chain can engender the formation of electronic states that promote electron spin delocalization. Second, considering the low reduction potential of NaAsc ($E^{-/0} = -0.290$ V), the electron transfer to vacant states characterized by more negative reduction potentials is thermodynamically unfavorable and may be characterized by a low electron transfer rate constant.

4. CONCLUSIONS

In conclusion, we report the synthesis and structural and electronic characterization of two water-soluble naphthalene diimide oligomers that feature different chemical linkages. Using ground-state electronic absorption spectroscopy, we show that the flexible chains of the oligomer enforce electronic coupling between NDI units evidencing the spectroscopic properties of H-like aggregates. Cyclic voltammetry experi-

https://doi.org/10.1021/acs.jpcc.1c02239
J. Phys. Chem. C 2021, 125, 10526−10538

ments reveal the role of chemical linkages in dictating the potentiometric properties of the oligomers, where the $(\mathbf{NDI\text{-}Am})_5$ derivative demonstrates a first reduction potential ($E^{(i)}$ = −0.025 V vs SCE) stabilized by more than 200 meV as compared to that of its $(\mathbf{NDI\text{-}Triazo})_5$ analogue ($E^{(i)}$ = −0.250 V vs SCE). The low-lying reduction potentials enabled the use of sodium ascorbate and sodium hydrosulfide as sacrificial electron donors to probe the spectroscopic properties of the n-doped states. The detection of absorptive features reminiscent of those observed in covalent NDI dimers indicates the formation of n-doped states characterized by a non-negligible degree of NDI π−anion interactions. TD-DFT calculations further corroborate this hypothesis.

To further elucidate the electron spin properties of the n-doped state, EPR spectroscopy experiments were performed on the $(\mathbf{NDI\text{-}Am})_5$ oligomer. These measurements and their analyses highlight the existence of localized and delocalized unpaired electron spin densities that can be controlled by the oxidation potential of the sacrificial electron donors used to n-dope the oligomer chain. Overall, this study highlights the existence of energetically disparate n-doped states governed by the chemical linkages that tether the redox-active NDI units in the oligomer chain. The development and characterization of water-soluble oligomers, whose structure−function relationships can be tuned using chemical stimuli, pave the way to engineer hydrophilic materials relevant to photonic, chemical sensing, and transducing applications.

■ ASSOCIATED CONTENT

Supporting Information

The Supporting Information is available free of charge at https://pubs.acs.org/doi/10.1021/acs.jpcc.1c02239.

Synthesis, sample preparation, cyclic voltammograms, XPS spectra, NMR spectra, IR spectra, and MS spectra (PDF)

■ AUTHOR INFORMATION

Corresponding Authors

Katlyn Meier − *Department of Chemistry, University of Miami, Coral Gables, Florida 33146, United States*; Phone: +1 305 284 9807; Email: kmeier@miami.edu

Jean-Hubert Olivier − *Department of Chemistry, University of Miami, Coral Gables, Florida 33146, United States*; orcid.org/0000-0003-0978-4107; Phone: +1 305 284 3279; Email: jh.olivier@miami.edu

Authors

Victor Paulino − *Department of Chemistry, University of Miami, Coral Gables, Florida 33146, United States*

Arindam Mukhopadhyay − *Department of Chemistry, University of Miami, Coral Gables, Florida 33146, United States*; orcid.org/0000-0002-0620-4157

Ifigeneia Tsironi − *Department of Chemistry, University of Miami, Coral Gables, Florida 33146, United States*

Kaixuan Liu − *Department of Chemistry, University of Miami, Coral Gables, Florida 33146, United States*

Dalia Husainy − *Department of Chemistry, University of Miami, Coral Gables, Florida 33146, United States*

Chuan Liu − *Department of Chemistry, University of Miami, Coral Gables, Florida 33146, United States*

Complete contact information is available at: https://pubs.acs.org/10.1021/acs.jpcc.1c02239

Author Contributions

The manuscript was written through contributions of all authors. All authors have given approval to the final version of the manuscript.

Notes

The authors declare no competing financial interest.

■ ACKNOWLEDGMENTS

This work is supported by the National Science Foundation under the CAREER award CHE-1941410. Additional support provided to J.-H.O. by the Arnold and Mabel Beckman Foundation under the award Beckman Young Investigator Award 2018 is acknowledged. K.K.M. is thankful to the University of Miami. The authors thank Dr. Donley at the University of North Carolina at Chapel Hill for her assistance with XPS characterization, Prof. Leblanc for his assistance with AFM, and Prof. Sean Roberts at UT Austin for his helpful discussion regarding fitting the NIR transitions. The authors are grateful to the Institute for Data Science and Computing at the University of Miami for providing access to Pegasus supercomputer and to BioNIUM, especially Dr. Kim for his assistance with SEM.

■ REFERENCES

(1) Susumu, K.; Therien, M. J. Decoupling Optical and Potentiometric Band Gaps in π-Conjugated Materials. *J. Am. Chem. Soc.* **2002**, *124*, 8550−8552.

(2) Deria, P.; Olivier, J.-H.; Park, J.; Therien, M. J. Potentiometric, Electronic, and Transient Absorptive Spectroscopic Properties of Oxidized Single-Walled Carbon Nanotubes Helically Wrapped by Ionic, Semiconducting Polymers in Aqueous and Organic Media. *J. Am. Chem. Soc.* **2014**, *136*, 14193−14199.

(3) Ostroverkhova, O. Organic Optoelectronic Materials: Mechanisms and Applications. *Chem. Rev.* **2016**, *116*, 13279−13412.

(4) Olshansky, J. H.; Harvey, S. M.; Pennel, M. L.; Krzyaniak, M. D.; Schaller, R. D.; Wasielewski, M. R. Using Photoexcited Core/Shell Quantum Dots To Spin Polarize Appended Radical Qubits. *J. Am. Chem. Soc.* **2020**, *142*, 13590−13597.

(5) Olshansky, J. H.; Zhang, J.; Krzyaniak, M. D.; Lorenzo, E. R.; Wasielewski, M. R. Selectively Addressable Photogenerated Spin Qubit Pairs in DNA Hairpins. *J. Am. Chem. Soc.* **2020**, *142*, 3346−3350.

(6) Schenning, A. P. H. J.; Meijer, E. W. Supramolecular electronics; nanowires from self-assembled [small pi]-conjugated systems. *Chem. Commun.* **2005**, *419*, 3245−3258.

(7) De Greef, T. F. A.; Smulders, M. M. J.; Wolffs, M.; Schenning, A. P. H. J.; Sijbesma, R. P.; Meijer, E. W. Supramolecular Polymerization. *Chem. Rev.* **2009**, *109*, 5687−5754.

(8) Yang, L.; Tan, X.; Wang, Z.; Zhang, X. Supramolecular Polymers: Historical Development, Preparation, Characterization, and Functions. *Chem. Rev.* **2015**, *115*, 7196−7239.

(9) Wehner, M.; Würthner, F. Supramolecular polymerization through kinetic pathway control and living chain growth. *Nat. Rev. Chem.* **2020**, *4*, 38−53.

(10) Armao, J. J.; Rabu, P.; Moulin, E.; Giuseppone, N. Long-Range Energy Transport via Plasmonic Propagation in a Supramolecular Organic Waveguide. *Nano Lett.* **2016**, *16*, 2800−2805.

(11) Wan, Y.; Stradomska, A.; Knoester, J.; Huang, L. Direct Imaging of Exciton Transport in Tubular Porphyrin Aggregates by Ultrafast Microscopy. *J. Am. Chem. Soc.* **2017**, *139*, 7287−7293.

(12) Liess, A.; Lv, A.; Arjona-Esteban, A.; Bialas, D.; Krause, A.-M.; Stepanenko, V.; Stolte, M.; Würthner, F. Exciton Coupling of Merocyanine Dyes from H- to J-type in the Solid State by Crystal Engineering. *Nano Lett.* **2017**, *17*, 1719−1726.

(13) Jin, X.-H.; Price, M. B.; Finnegan, J. R.; Boott, C. E.; Richter, J. M.; Rao, A.; Menke, S. M.; Friend, R. H.; Whittell, G. R.; Manners, I.

Long-range exciton transport in conjugated polymer nanofibers prepared by seeded growth. *Science* **2018**, *360*, 897−900.
(14) Liu, C.; Liu, K.; Mukhopadhyay, A.; Paulino, V.; Bernard, B.; Olivier, J.-H. Butadiyne-Bridged (Porphinato)Zinc(II) Chromophores Assemble into Free-Standing Nanosheets. *Organometallics* **2020**, *39*, 2984−2990.
(15) Singh, V.; Zoric, M. R.; Hargenrader, G. N.; Valentine, A. J. S.; Zivojinovic, O.; Milic, D. R.; Li, X.; Glusac, K. D. Exciton Coherence Length and Dynamics in Graphene Quantum Dot Assemblies. *J. Phys. Chem. Lett.* **2020**, *11*, 210−216.
(16) Weldeab, A. O.; Steen, A.; Starkenburg, D. J.; Williams, J. S. D.; Abboud, K. A.; Xue, J.; Hammer, N. I.; Castellano, R. K.; Watkins, D. L. Tuning the structural and spectroscopic properties of donor−acceptor−donor oligomers via mutual X-bonding, H-bonding, and $\pi-\pi$ interactions. *J. Mater. Chem. C* **2018**, *6*, 11992−12000.
(17) Liu, C.; Liu, K.; Klutke, J.; Ashcraft, A.; Steefel, S.; Olivier, J.-H. Deciphering the potentiometric properties of (porphinato)zinc(ii)-derived supramolecular polymers and related superstructures. *J. Mater. Chem. C* **2018**, *6*, 11980−11991.
(18) Ashcraft, A.; Liu, K.; Mukhopadhyay, A.; Paulino, V.; Liu, C.; Bernard, B.; Husainy, D.; Phan, T.; Olivier, J.-H. A Molecular Strategy to Lock-in the Conformation of a Perylene Bisimide-Derived Supramolecular Polymer. *Angew. Chem., Int. Ed.* **2020**, *59*, 7487−7493.
(19) Mukhopadhyay, A.; Paulino, V.; Liu, K.; Donley, C. L.; Bernard, B.; Shomar, A.; Liu, C.; Olivier, J.-H. Leveraging the Assembly of a Rylene Dye to Tune the Semiconducting Properties of Functionalized n-Type, Hybrid Si Interfaces. *ACS Appl. Mater. Interfaces* **2021**, *13*, 4665−4675.
(20) Liu, K.; Paulino, V.; Mukhopadhyay, A.; Bernard, B.; Kumbhar, A.; Liu, C.; Olivier, J.-H. How to reprogram the excitonic properties and solid-state morphologies of π-conjugated supramolecular polymers. *Phys. Chem. Chem. Phys.* **2021**, *23*, 2703−2714.
(21) Spano, F. C.; Silva, C. H- and J-Aggregate Behavior in Polymeric Semiconductors. *Annu. Rev. Phys. Chem.* **2014**, *65*, 477−500.
(22) Hestand, N. J.; Spano, F. C. Molecular Aggregate Photophysics beyond the Kasha Model: Novel Design Principles for Organic Materials. *Acc. Chem. Res.* **2017**, *50*, 341−350.
(23) Hestand, N. J.; Spano, F. C. Expanded Theory of H- and J-Molecular Aggregates: The Effects of Vibronic Coupling and Intermolecular Charge Transfer. *Chem. Rev.* **2018**, *118*, 7069−7163.
(24) Coropceanu, V.; Cornil, J.; da Silva Filho, D. A.; Olivier, Y.; Silbey, R.; Brédas, J.-L. Charge Transport in Organic Semiconductors. *Chem. Rev.* **2007**, *107*, 926−952.
(25) Hill, D. J.; Mio, M. J.; Prince, R. B.; Hughes, T. S.; Moore, J. S. A Field Guide to Foldamers. *Chem. Rev.* **2001**, *101*, 3893−4012.
(26) Kataoka, Y.; Kanbayashi, N.; Fujii, N.; Okamura, T.-a.; Haino, T.; Onitsuka, K. Construction of Helically Stacked π-Electron Systems in Poly(quinolylene-2,3-methylene) Stabilized by Intramolecular Hydrogen Bonds. *Angew. Chem., Int. Ed.* **2020**, *59*, 10286−10291.
(27) Méndez-Ardoy, A.; Markandeya, N.; Li, X.; Tsai, Y.-T.; Pecastaings, G.; Buffeteau, T.; Maurizot, V.; Muccioli, L.; Castet, F.; Huc, I.; et al. Multi-dimensional charge transport in supramolecular helical foldamer assemblies. *Chem. Sci.* **2017**, *8*, 7251−7257.
(28) Carini, M.; Ruiz, M. P.; Usabiaga, I.; Fernández, J. A.; Cocinero, E. J.; Melle-Franco, M.; Diez-Perez, I.; Mateo-Alonso, A. High conductance values in π-folded molecular junctions. *Nat. Commun.* **2017**, *8*, No. 15195.
(29) Li, X.; Markandeya, N.; Jonusauskas, G.; McClenaghan, N. D.; Maurizot, V.; Denisov, S. A.; Huc, I. Photoinduced Electron Transfer and Hole Migration in Nanosized Helical Aromatic Oligoamide Foldamers. *J. Am. Chem. Soc.* **2016**, *138*, 13568−13578.
(30) Han, J. J.; Wang, W.; Li, A. D. Q. Folding and Unfolding of Chromophoric Foldamers Show Unusual Colorful Single Molecule Spectral Dynamics. *J. Am. Chem. Soc.* **2006**, *128*, 672−673.
(31) George, K. L.; Horne, W. S. Foldamer Tertiary Structure through Sequence-Guided Protein Backbone Alteration. *Acc. Chem. Res.* **2018**, *51*, 1220−1228.
(32) Burattini, S.; Colquhoun, H. M.; Fox, J. D.; Friedmann, D.; Greenland, B. W.; Harris, P. J. F.; Hayes, W.; Mackay, M. E.; Rowan, S. J. A self-repairing, supramolecular polymer system: healability as a consequence of donor−acceptor $\pi-\pi$ stacking interactions. *Chem. Commun.* **2009**, 6717−6719.
(33) Scott Lokey, R.; Iverson, B. L. Synthetic molecules that fold into a pleated secondary structure in solution. *Nature* **1995**, *375*, 303−305.
(34) Zych, A. J.; Iverson, B. L. Synthesis and Conformational Characterization of Tethered, Self-Complexing 1,5-Dialkoxynaphthalene/1,4,5,8-Naphthalenetetracarboxylic Diimide Systems. *J. Am. Chem. Soc.* **2000**, *122*, 8898−8909.
(35) Lokey, R. S.; Kwok, Y.; Guelev, V.; Pursell, C. J.; Hurley, L. H.; Iverson, B. L. A New Class of Polyintercalating Molecules. *J. Am. Chem. Soc.* **1997**, *119*, 7202−7210.
(36) Faour, L.; Adam, C.; Gautier, C.; Goeb, S.; Allain, M.; Levillain, E.; Canevet, D.; Sallé, M. Redox-controlled hybridization of helical foldamers. *Chem. Commun.* **2019**, *55*, 5743−5746.
(37) Zhang, D.-W.; Tian, J.; Chen, L.; Zhang, L.; Li, Z.-T. Dimerization of Conjugated Radical Cations: An Emerging Non-Covalent Interaction for Self-Assembly. *Chem. Asian J.* **2015**, *10*, 56−68.
(38) Miller, L. L.; Mann, K. R. π-Dimers and π-Stacks in Solution and in Conducting Polymers. *Acc. Chem. Res.* **1996**, *29*, 417−423.
(39) Spruell, J. M.; Coskun, A.; Friedman, D. C.; Forgan, R. S.; Sarjeant, A. A.; Trabolsi, A.; Fahrenbach, A. C.; Barin, G.; Paxton, W. F.; Dey, S. K.; et al. Highly stable tetrathiafulvalene radical dimers in [3]catenanes. *Nat. Chem.* **2010**, *2*, 870−879.
(40) Korevaar, P. A.; Kaplan, C. N.; Grinthal, A.; Rust, R. M.; Aizenberg, J. Non-equilibrium signal integration in hydrogels. *Nat. Commun.* **2020**, *11*, No. 386.
(41) Sorrenti, A.; Leira-Iglesias, J.; Markvoort, A. J.; de Greef, T. F. A.; Hermans, T. M. Non-equilibrium supramolecular polymerization. *Chem. Soc. Rev.* **2017**, *46*, 5476−5490.
(42) Grzybowski, B. A.; Huck, W. T. S. The nanotechnology of life-inspired systems. *Nat. Nanotechnol.* **2016**, *11*, 585−592.
(43) Singh, N.; Lainer, B.; Formon, G. J. M.; De Piccoli, S.; Hermans, T. M. Re-programming Hydrogel Properties Using a Fuel-Driven Reaction Cycle. *J. Am. Chem. Soc.* **2020**, *142*, 4083−4087.
(44) Bhosale, S. V.; Jani, C. H.; Langford, S. J. Chemistry of naphthalene diimides. *Chem. Soc. Rev.* **2008**, *37*, 331−342.
(45) Sakai, N.; Mareda, J.; Vauthey, E.; Matile, S. Core-substituted naphthalenediimides. *Chem. Commun.* **2010**, *46*, 4225−4237.
(46) Shukla, J.; Mukhopadhyay, P. Synthesis of Functionalized Naphthalene Diimides and their Redox Properties. *Eur. J. Org. Chem.* **2019**, *2019*, 7770−7786.
(47) Schmidt, S. B.; Biskup, T.; Jiao, X.; McNeill, C. R.; Sommer, M. Controlling intermolecular redox-doping of naphthalene diimides. *J. Mater. Chem. C* **2019**, *7*, 4466−4474.
(48) Tu, S.; Kim, S. H.; Joseph, J.; Modarelli, D. A.; Parquette, J. R. Self-Assembly of a Donor−Acceptor Nanotube. A Strategy To Create Bicontinuous Arrays. *J. Am. Chem. Soc.* **2011**, *133*, 19125−19130.
(49) Sforazzini, G.; Orentas, E.; Bolag, A.; Sakai, N.; Matile, S. Toward Oriented Surface Architectures with Three Coaxial Charge-Transporting Pathways. *J. Am. Chem. Soc.* **2013**, *135*, 12082−12090.
(50) Sanders, A. M.; Magnanelli, T. J.; Bragg, A. E.; Tovar, J. D. Photoinduced Electron Transfer within Supramolecular Donor−Acceptor Peptide Nanostructures under Aqueous Conditions. *J. Am. Chem. Soc.* **2016**, *138*, 3362−3370.
(51) Wu, Y.-L.; Horwitz, N. E.; Chen, K.-S.; Gomez-Gualdron, D. A.; Luu, N. S.; Ma, L.; Wang, T. C.; Hersam, M. C.; Hupp, J. T.; Farha, O. K.; et al. G-quadruplex organic frameworks. *Nat. Chem.* **2017**, *9*, 466−472.
(52) Guha, S.; Goodson, F. S.; Corson, L. J.; Saha, S. Boundaries of Anion/Naphthalenediimide Interactions: From Anion-π Interactions

to Anion-Induced Charge-Transfer and Electron-Transfer Phenomena. *J. Am. Chem. Soc.* **2012**, *134*, 13679−13691.
(53) Tam, T. L. D.; Xu, J. W. The role of fluoride in anion−π interaction with naphthalene diimide. *Chem. Commun.* **2019**, *55*, 6225−6228.
(54) Rananaware, A.; Samanta, M.; Bhosale, R. S.; Kobaisi, M. A.; Roy, B.; Bheemireddy, V.; Bhosale, S. V.; Bandyopadhyay, S.; Bhosale, S. V. Photomodulation of fluoride ion binding through anion-π interactions using a photoswitchable azobenzene system. *Sci. Rep.* **2016**, *6*, No. 22928.
(55) Šolomek, T.; Powers-Riggs, N. E.; Wu, Y.-L.; Young, R. M.; Krzyaniak, M. D.; Horwitz, N. E.; Wasielewski, M. R. Electron Hopping and Charge Separation within a Naphthalene-1,4:5,8-bis(dicarboximide) Chiral Covalent Organic Cage. *J. Am. Chem. Soc.* **2017**, *139*, 3348−3351.
(56) Beldjoudi, Y.; Narayanan, A.; Roy, I.; Pearson, T. J.; Cetin, M. M.; Nguyen, M. T.; Krzyaniak, M. D.; Alsubaie, F. M.; Wasielewski, M. R.; Stupp, S. I.; et al. Supramolecular Tessellations by a Rigid Naphthalene Diimide Triangle. *J. Am. Chem. Soc.* **2019**, *141*, 17783−17795.
(57) He, T.; Stolte, M.; Burschka, C.; Hansen, N. H.; Musiol, T.; Kälblein, D.; Pflaum, J.; Tao, X.; Brill, J.; Würthner, F. Single-crystal field-effect transistors of new Cl2-NDI polymorph processed by sublimation in air. *Nat. Commun.* **2015**, *6*, No. 5954.
(58) Mukhopadhyay, A.; Bernard, B.; Liu, K.; Paulino, V.; Liu, C.; Donley, C.; Olivier, J.-H. Molecular Strategies to Modulate the Electrochemical Properties of P-Type Si(111) Surfaces Covalently Functionalized with Ferrocene and Naphthalene Diimide. *J. Phys. Chem. B* **2019**, *123*, 11026−11041.
(59) Wu, Y.; Frasconi, M.; Gardner, D. M.; McGonigal, P. R.; Schneebeli, S. T.; Wasielewski, M. R.; Stoddart, J. F. Electron Delocalization in a Rigid Cofacial Naphthalene-1,8:4,5-bis-(dicarboximide) Dimer. *Angew. Chem., Int. Ed.* **2014**, *53*, 9476−9481.
(60) Penneau, J. F.; Stallman, B. J.; Kasai, P. H.; Miller, L. L. An imide anion radical that dimerizes and assembles into.pi.-stacks in solution. *Chem. Mater.* **1991**, *3*, 791−796.
(61) Takai, A.; Yasuda, T.; Ishizuka, T.; Kojima, T.; Takeuchi, M. A Directly Linked Ferrocene−Naphthalenediimide Conjugate: Precise Control of Stacking Structures of π-Systems by Redox Stimuli. *Angew. Chem., Int. Ed.* **2013**, *52*, 9167−9171.
(62) Liu, K.; Levy, A.; Liu, C.; Olivier, J.-H. Tuning Structure−Function Properties of π-Conjugated Superstructures by Redox-Assisted Self-Assembly. *Chem. Mater.* **2018**, *30*, 2143−2150.
(63) Liu, K.; Mukhopadhyay, A.; Ashcraft, A.; Liu, C.; Levy, A.; Blackwelder, P.; Olivier, J.-H. Reconfiguration of π-conjugated superstructures enabled by redox-assisted assembly. *Chem. Commun.* **2019**, *55*, 5603−5606.
(64) Kaufmann, C.; Bialas, D.; Stolte, M.; Würthner, F. Discrete π-Stacks of Perylene Bisimide Dyes within Folda-Dimers: Insight into Long- and Short-Range Exciton Coupling. *J. Am. Chem. Soc.* **2018**, *140*, 9986−9995.
(65) Espinoza, E. M.; Clark, J. A.; Soliman, J.; Derr, J. B.; Morales, M.; Vullev, V. I. Practical Aspects of Cyclic Voltammetry: How to Estimate Reduction Potentials when Irreversibility Prevails. *J. Electrochem. Soc.* **2019**, *166*, H3175.
(66) Avestro, A.-J.; Gardner, D. M.; Vermeulen, N. A.; Wilson, E. A.; Schneebeli, S. T.; Whalley, A. C.; Belowich, M. E.; Carmieli, R.; Wasielewski, M. R.; Stoddart, J. F. Gated Electron Sharing Within Dynamic Naphthalene Diimide-Based Oligorotaxanes. *Angew. Chem., Int. Ed.* **2014**, *53*, 4442−4449.
(67) Zhong, C. J.; Kwan, W. S. V.; Miller, L. L. Self-assembly of delocalized.pi.-stacks in solution. Assessment of structural effects. *Chem. Mater.* **1992**, *4*, 1423−1428.
(68) Stoll, S.; Schweiger, A. EasySpin, a comprehensive software package for spectral simulation and analysis in EPR. *J. Magn. Reson.* **2006**, *178*, 42−55.

https://doi.org/10.1021/acs.jpcc.1c02239
J. Phys. Chem. C 2021, 125, 10526−10538